Developmental Cell
Article

Rab25 Associates with α5β1 Integrin to Promote Invasive Migration in 3D Microenvironments

Patrick T. Caswell,[1] Heather J. Spence,[1] Maddy Parsons,[2] Dominic P. White,[1] Katherine Clark,[3] Kwai Wa Cheng,[4] Gordon B. Mills,[4] Martin J. Humphries,[5] Anthea J. Messent,[5] Kurt I. Anderson,[1] Mary W. McCaffrey,[6] Bradford W. Ozanne,[1] and Jim C. Norman[1,*]

[1]Beatson Institute for Cancer Research, Garscube Estate, Switchback Road, Bearsden, Glasgow G61 1BD, UK
[2]Randall Centre, King's College London, Guy's Medical School Campus, London SE1 1UL, UK
[3]Department of Biochemistry, Henry Wellcome Building, University of Leicester, Lancaster Road, Leicester LE1 9HN, UK
[4]Department of Molecular Therapeutics, University of Texas MD Anderson Cancer Center, Houston, TX 77054, USA
[5]Wellcome Trust Centre for Cell-Matrix Research, Faculty of Life Sciences, University of Manchester, Michael Smith Building, Oxford Road, Manchester, M13 9PT, UK
[6]Molecular Cell Biology Laboratory, Department of Biochemistry, Biosciences Institute, University College Cork, Cork, Ireland
*Correspondence: j.norman@beatson.gla.ac.uk
DOI 10.1016/j.devcel.2007.08.012

SUMMARY

Here, we report a direct interaction between the β1 integrin cytoplasmic tail and Rab25, a GTPase that has been linked to tumor aggressiveness and metastasis. Rab25 promotes a mode of migration on 3D matrices that is characterized by the extension of long pseudopodia, and the association of the GTPase with α5β1 promotes localization of vesicles that deliver integrin to the plasma membrane at pseudopodial tips as well as the retention of a pool of cycling α5β1 at the cell front. Furthermore, Rab25-driven tumor-cell invasion into a 3D extracellular matrix environment is strongly dependent on ligation of fibronectin by α5β1 integrin and the capacity of Rab25 to interact with β1 integrin. These data indicate that Rab25 contributes to tumor progression by directing the localization of integrin-recycling vesicles and thereby enhancing the ability of tumor cells to invade the extracellular matrix.

INTRODUCTION

Rab proteins are members of the Ras superfamily of GTPases that are involved in membrane-trafficking events. The Rab11 subfamily, comprised of Rab11a, Rab11b, and Rab25 (also known as Rab11c), controls the return of internalized membrane-associated moieties to the cell surface (Zerial and McBride, 2001), and data pointing to the possibility that Rab11 pathways contribute to aspects of tumorogenicity are accumulating (Garcia et al., 2005; Gebhardt et al., 2005; Gress et al., 1996; Natrajan et al., 2006; Ray et al., 1997, 2004). Recently, Rab25, which is restricted to an epithelial expression profile, unlike the ubiquitous Rab11s (Rab11a and Rab11b) in normal tissue (Goldenring et al., 1993), has been shown to increase the aggressiveness of ovarian and breast tumors both clinically and in mouse models (Cheng et al., 2004). Furthermore, the fact that Rab25 is a component of the invasive signature of breast cancer cells in vivo and in vitro (Wang et al., 2004) stresses the need to further our understanding of Rab25-mediated trafficking events in transformed cells, and how these may contribute to metastatic progression.

Integrins are heterodimeric extracellular matrix (ECM) receptors involved in multiple aspects of cell behavior in physiological and pathological contexts (Hynes, 2002). Many integrins are continually internalized from the plasma membrane into endosomal compartments and are subsequently recycled (Caswell and Norman, 2006; Pellinen et al., 2006), and it is probable that such endo-/exocytic cycling acts to coordinate the functionality of integrins and other ECM receptors. Indeed, Rab4 and Rab11 regulate the recycling of a range of integrins, including α5β1, αvβ3, α6β1, α6β4, and αLβ2 (Fabbri et al., 2005; Powelka et al., 2004; Roberts et al., 2001, 2004; Strachan and Condic, 2004; Woods et al., 2004; Yoon et al., 2005), and disruption of recycling via the Rab11 compartment has been shown to compromise integrin-dependent cell spreading and migration (Caswell and Norman, 2006; Jones et al., 2006).

α5β1 is known to influence tumor-cell survival, proliferation, and metastasis (Akiyama et al., 1995; Danen and Yamada, 2001), and its action can be both oncogenic and tumor suppressive, depending on cell type and origin. Furthermore, α5β1 and its ligand fibronectin (FN) are known to be present in a range of cellular structures such as focal adhesions, focal complexes, fibrillar, and 3D matrix adhesions, which can make stimulatory and inhibitory contributions to cell migration in both 3D and 2D matrices (Cukierman et al., 2001; Pankov et al., 2000; Zamir et al., 1999). Indeed, FN is an abundant ECM protein found in most types of connective/interstitial tissue; therefore, the ability of cells to migrate through FN-containing matrices is critical to metastatic development. Given the diverse and sometimes opposing modes of action of the

cell's major FN-binding integrin, it would be interesting to determine whether a Rab GTPase with a proven link to tumor progression could influence α5β1 function such that tumorogenesis and/or invasive migration were favored.

Here, we report an interaction, which is both selective and direct, between the β1 integrin cytoplasmic tail and a GTPase of the Rab family, Rab25. Rab25 promotes an invasive mode of migration on 3D matrices in which it functions to localize and keep α5β1 at the tips of extending pseudopodia. Furthermore, Rab25-driven tumor-cell invasion is strongly dependent on FN, α5β1, and the ability of Rab25 to interact with β1 integrin. We propose that Rab25 contributes to tumor progression by enhancing the ability of tumor cells to invade FN-containing ECM and form metastases.

RESULTS

Rab25 Directly Associates with β1 Integrin in a GTP-Dependent Manner

Upon isolation of Rab25 from A2780 cells stably expressing HA-Rab25 by immunoprecipitation of the HA tag, we found that β1 integrin efficiently coprecipitated with Rab25 (Figure 1A). We could not, however, detect the presence of other cycling integrins, e.g., αvβ3 in these HA-Rab25 immunoprecipitates (data not shown). Robust coimmunoprecipitation of Rab25 and integrin was also observed when the α5 subunit of the integrin heterodimer was immunoprecipitated (Figure 1B). Furthermore, this association was Rab25 specific, as no other Rab11 family member (neither Rab11a nor Rab11b) coimmunoprecipitated with α5β1 (Figure 1B).

We further investigated the nature of this interaction by using a GST pull-down strategy. While GST and GST-α5 cytotail-coated beads were unable to pull down Rab25 from cell lysates, the GST-β1 cytotail efficiently captured Rab25 (Figure 1C), indicating that the β1 integrin subunit mediates the association with Rab25. Furthermore, the selectivity of the interaction among Rab11 family members was confirmed, as the GST-β1 cytotail did not recruit Rab11a/b from cell lysates (Figure 1C). Using bacterially expressed recombinant His-Rab25 and recombinant GST-α5 and -β1 integrin cytotails, we further characterized the nature of Rab25-integrin association. Purified Rab25 preloaded with GDP showed little affinity for the GST-β1 cytotail (Figure 1D). However, when Rab25 was presented to the β1-cytotail in its GTP-bound "active" form, there was a vast increase in the affinity of Rab25 for integrin (Figure 1D).

To further establish a direct link between β1 integrin and Rab25, GFP-β1 integrin and Cherry-Rab25 were expressed in β1−/− mouse embryo fibroblasts (MEFs) and imaged by multiphoton fluorescence lifetime imaging microscopy (FLIM). GFP fluorescence normally undergoes a single exponential decay, but if fluorescence resonance energy transfer (FRET) to an acceptor fluorophore (in this case Cherry-Rab25) occurs, this shortens the fluorescence lifetime of the donor (GFP-β1). Fluorescence lifetime maps show a clear reduction in the lifetime of GFP-β1 fluorescence in cells expressing Cherry-Rab25, indicating that FRET was occurring between β1 integrin and Rab25, but not with Rab11a (Figure 1E) even though the two Rab GTPases were expressed at similar levels (Figure 1E, center panels). Interestingly, this reduction in lifetime was concentrated in puncta close to the plasma membrane, indicating that association between Rab25 and the integrin may occur in that area of the cell. Quantitation of FRET efficiency between GFP-β1 and the Cherry-Rabs clearly indicates that Rab25 does indeed bind β1 integrin within the cell, whereas Rab11a does not (Figure 1E).

Complete (Rab25>11L) or partial (Rab25>11S; Rab25/11/25) replacement of the hypervariable Rab25 C terminus with the corresponding region of Rab11a completely abrogated the ability of Rab25 to associate with β1 integrin, indicating that the amino acids of Rab25 involved in the direct interaction with β1 integrin lie within this region (Figure 2). Conversely, replacement of the Rab11a C terminus with the corresponding region of Rab25 (Rab11>25L) conferred β1-binding capacity to Rab11a, although replacement of subdomains of the hypervariable region did not enable β1 binding in Rab11a (Figure 2). Taken together, these data demonstrate that the direct interaction of Rab25 with β1 integrin is mediated by the hypervariable C-terminal region of Rab25.

Rab25 Promotes α5β1-Dependent Migration in 3D

We did not detect differences in the characteristics of A2780 cell migration (speed, persistence, directionality, and formation of leading lamellae) on plastic surfaces after expression of Rab25 (Figure S1; see the Supplemental Data available with this article online), indicating that this GTPase is unlikely to form part of the minimal motility machine or to regulate basic processes of cell migration such as actin polymerization or the recruitment of integrins to focal complexes. However, there are key differences between the characteristics of cells migrating in 3D versus on 2D matrices (Even-Ram and Yamada, 2005), and experimental systems measuring migration across plastic surfaces may not accurately model the type of motility that would be deployed by a tumor cell to move away from the primary tumor and form metastases at distant sites. To elucidate the potential contribution that Rab25 makes to the invasive phenotype of aggressive tumors, we employed an inverted invasion assay, in which cells must migrate upward through either matrigel (predominantly a mixture of the ECM components laminin and collagen IV) or gels formed from fibrillar type I collagen. A2780-DNA3 cells showed little invasive activity when presented with either of these 3D environments, and supplementing the gels with exogenous FN prior to plug polymerization resulted in only a small increase in invasion though matrigel (Figure 3A) and no change in migration through type I collagen (Figure 3B). A2780 cells stably expressing Rab25 invaded type I collagen or matrigel to a modest level, but, crucially, this was strongly potentiated when exogenous FN was added (Figures 3A and 3B). Transient expression of GFP-Rab25, compared with

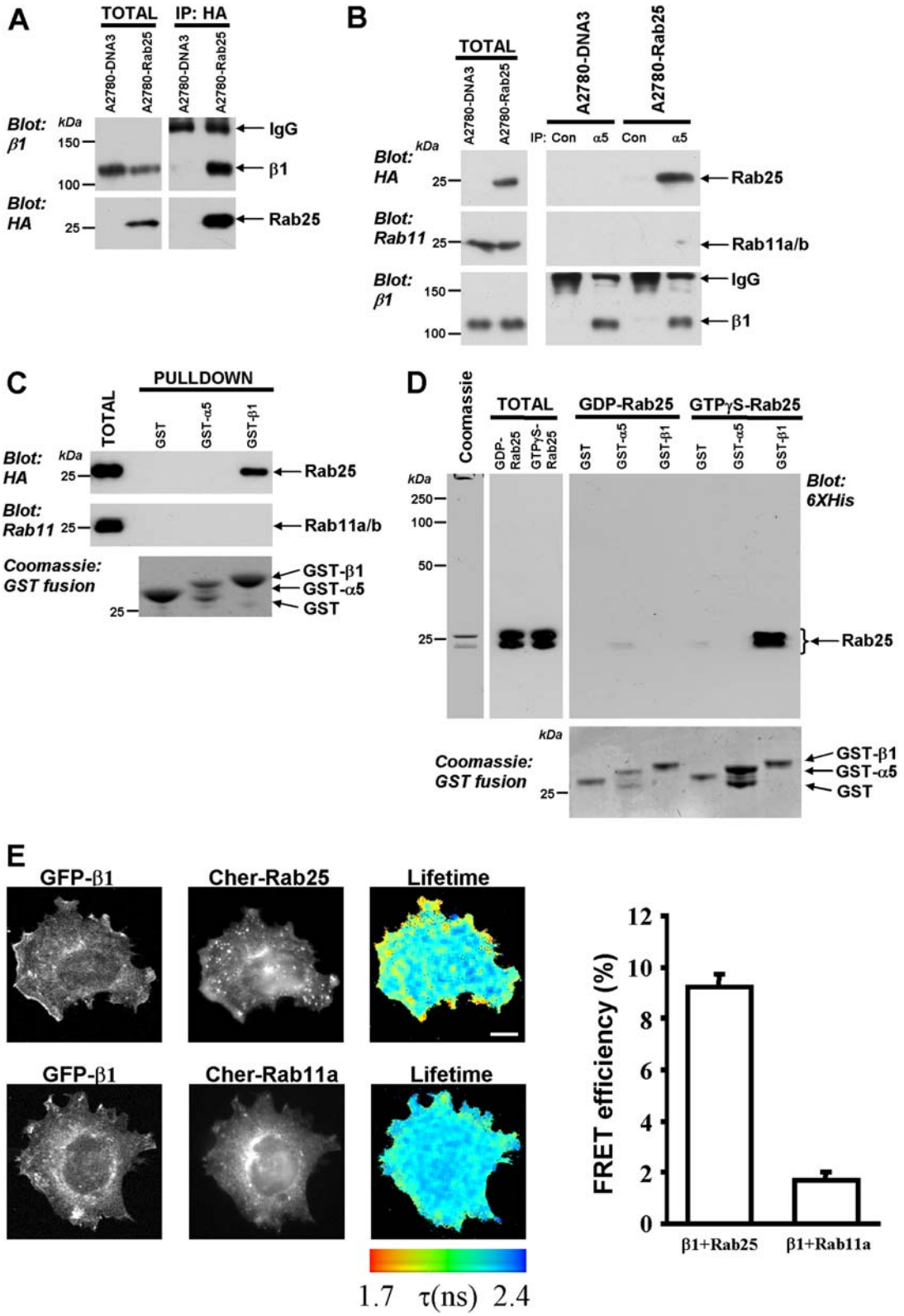

Figure 1. α5β1 Integrin Interacts with Rab25 via a GTP-Dependent Association with the β1 Cytodomain

(A) Rab25 was immunoprecipitated from lysates of A2780 cells stably expressing HA-Rab25 (A2780-Rab25) or empty control vector (A2780-DNA3) with a monoclonal anti-HA antibody (12CA5) and was analyzed for the presence of Rab25 (HA) and β1 integrin by immunoblotting.

GFP or GFP-Rab11a, also significantly enhanced A2780 cell invasion into a FN-rich matrix (Figure 3C). Importantly, RNAi of Rab25 (Figure 3E) significantly blocked the FN-dependent invasiveness of A2780-Rab25 cells (Figure 3D).

Use of blocking antibodies further established the requirement for the α5β1-FN ligand pair in Rab25-mediated invasion. P1F6, an αvβ5-blocking antibody, had no effect on the invasion of Rab25-expressing A2780 cells into FN-containing matrigel (Figure 3D). Antibodies that specifically block the α5 subunit of the integrin heterodimer (mAb16) or the α5β1-binding site in FN (16G3) both significantly reduced the degree of invasion to a level comparable to that seen in A2780-Rab25 cells in the absence of added FN (compare Figure 3D with Figure 3A), confirming the importance of α5β1 ligation in Rab25-mediated invasion. Furthermore, blockade of the β1 integrin subunit with mAb13 effected a more profound inhibition of invasiveness than did inhibition of α5 integrin or FN alone (Figure 3D), indicating that Rab25-α5β1 forms part of a program that confers FN-dependent invasive migration to A2780 cells, but that this process also requires ligation of other β1 integrins.

We deployed the Rab25/11 domain-swap chimeras (Figure 2B) to further test the requirement for α5β1 association in Rab25-driven invasion. Rab25>11L, which does not interact with β1 integrin, did not promote invasion, nor did Rab11a (Figure 3C). Conversely, the β1-interacting GFP-Rab11>25L enhanced invasive activity to a similar extent as Rab25 (Figure 3C), indicating that Rab25 promotes the invasive capacity of cells in a manner dependent on its ability to associate directly with β1 integrin.

Many reports describe FN as anti-invasive and antimetastatic and indicate that it may act as a tumor suppressor under certain circumstances (Hynes, 1976; Spence et al., 2006; Vaheri and Mosher, 1978; Yamada and Olden, 1978). Indeed, after transfection of the FBR v-fos oncogene, 208F rat fibroblasts (FBR cells) transform morphologically and acquire a highly motile and invasive phenotype characterized by extension of long pseudopodia emanating from a bipolar spindle-shaped cell body, and there is a dramatic downregulation of FN (Curran and Verma, 1984; Hennigan et al., 1994; McGarry et al., 2004). In 3D matrices, these cells are very invasive and extend pseudopodial protrusions in the direction of invasive migration. Exposing FBR cells to FN by plating them on FN-coated coverslips or including FN in the 3D matrix

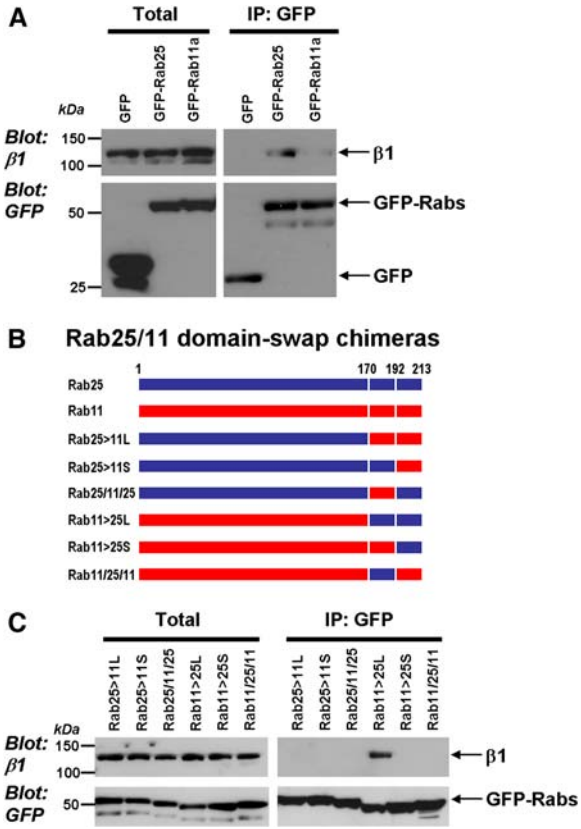

Figure 2. Association with α5β1 Integrin Is Mediated via the C-Terminal Region of Rab25

(A) A2780 cells expressing GFP-Rab25, GFP-Rab11a, or GFP alone were lysed, and these fusion proteins immunoprecipitated with an anti-GFP antibody. The resulting immunoprecipitates were screened for the presence of α5β1 by immunoblotting for the β1 integrin chain (upper panels). The loading of GFP was confirmed by western blot with anti-GFP (lower panels).

(B) Schematic representation and nomenclature of the Rab25/Rab11a domain-swap chimeras employed for the present study. Regions of Rab25 and Rab11a sequence are shown in blue and red, respectively.

(C) A2780 cells expressing the indicated GFP-tagged Rab25/Rab11a domain-swap chimeras were lysed, immunoprecipitated, and analyzed by western blot in a manner similar to that described in (A).

completely reverts the invasive migration to the normal 208F fibroblastic phenotype in an α5β1-dependent process (Spence et al., 2006) (Figures 4A and 4B). However,

(B) Lysates prepared as in (A) were immunoprecipitated with either monoclonal antibodies recognizing α5 integrin (α5) or an isotype-matched control antibody (Con). The presence of β1 integrin, Rab25 (HA), and Rab11a/b was detected by immunoblotting.

(C) Glutathione agarose beads bound to GST, GST-α5, or GST-β1 fusion proteins were incubated with lysates of COS-1 cells expressing HA-Rab25. The presence of Rab25 (HA) and Rab11a/b was detected by immunoblotting, and the loading of GST fusion proteins was confirmed by Coomassie staining.

(D) Glutathione agarose beads bound to GST or GST-integrin cytodomain fusion proteins were incubated with recombinant purified His-Rab25 that had been preloaded with either GDP (GDP-Rab25) or GTPγS (GTPγS-Rab25). The association of Rab25 was determined by immunoblotting, and loading of GST fusion proteins was confirmed by Coomassie staining. It should be noted that in these experiments, His-Rab25 resolves as two bands in SDS-PAGE. This is not owing to proteolysis, as mass spectrometric analysis has confirmed that both these forms of Rab25 possess intact amino and carboxy termini.

(E) β1 −/− fibroblasts expressing GFP-β1 integrin were transfected with Cherry-Rab25 or -Rab11a and were plated onto glass coverslips. Images show the GFP multiphoton intensity image and the corresponding wide-field CCD camera image of the GFP-β1 and Cherry-Rab GTPase expression levels. Lifetime images mapping spatial FRET across the cells are depicted with a pseudocolor scale (blue, normal lifetime; red, FRET). The scale bar is 10 μm. The graph depicts the average FRET efficiency over three independent experiments. Values are mean ± SEM, n = 12.

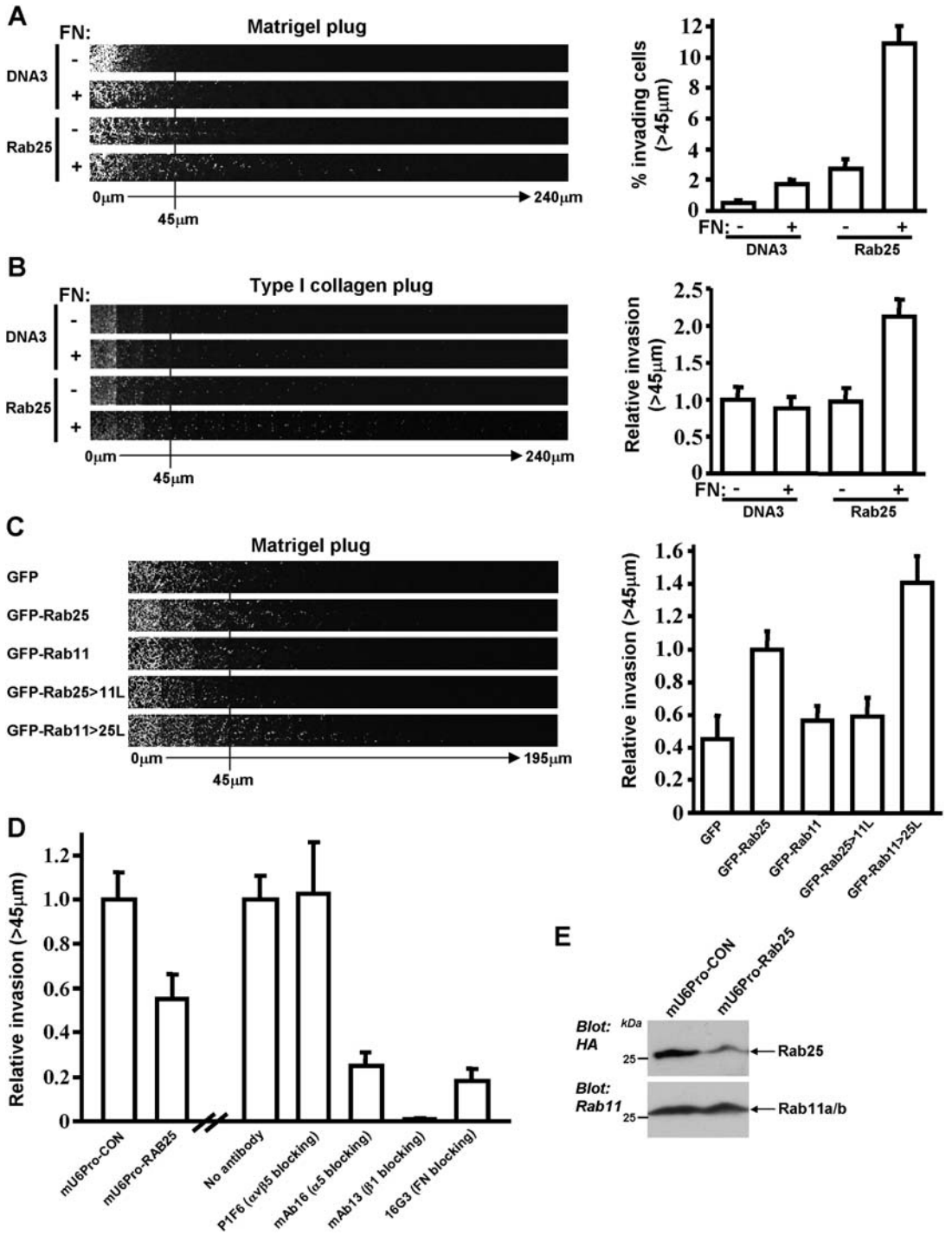

Figure 3. Rab25 Promotes α5β1-Fibronectin-Dependent Invasion of A2780 Cells

(A and B) Invasive migration of A2780 cells stably expressing Rab25 or empty vector (DNA3) into plugs of (A) matrigel or (B) type I collagen in the presence and absence of 25 μg/ml fibronectin (FN) was determined by using an inverted invasion assay. Invading cells were stained with Calcein-AM and were visualized by confocal microscopy. Serial optical sections were captured at 15 μm intervals and are presented as a sequence in which the individual optical sections are placed alongside one another with increasing depth from left to right, as indicated. Invasion assays were quantitated by measuring the fluorescence intensity of cells penetrating the matrigel to depths of 45 μm and greater; this intensity was expressed as (A) a percentage of the total fluorescence intensity of all cells within the plug or was expressed (B) relative to the levels observed for A2780-DNA3 cells in the absence of FN. Data represent mean ± SEM from three independent experiments.

(C) Invasive migration of A2780 cells expressing GFP, GFP-Rab25, GFP-Rab11a, GFP-Rab25>11L, and GFP-Rab11>25L into matrigel supplemented with FN was determined and quantified as in (B), but values were expressed relative to the levels observed for GFP-Rab25-driven invasion. Values are mean ± SEM from three independent experiments.

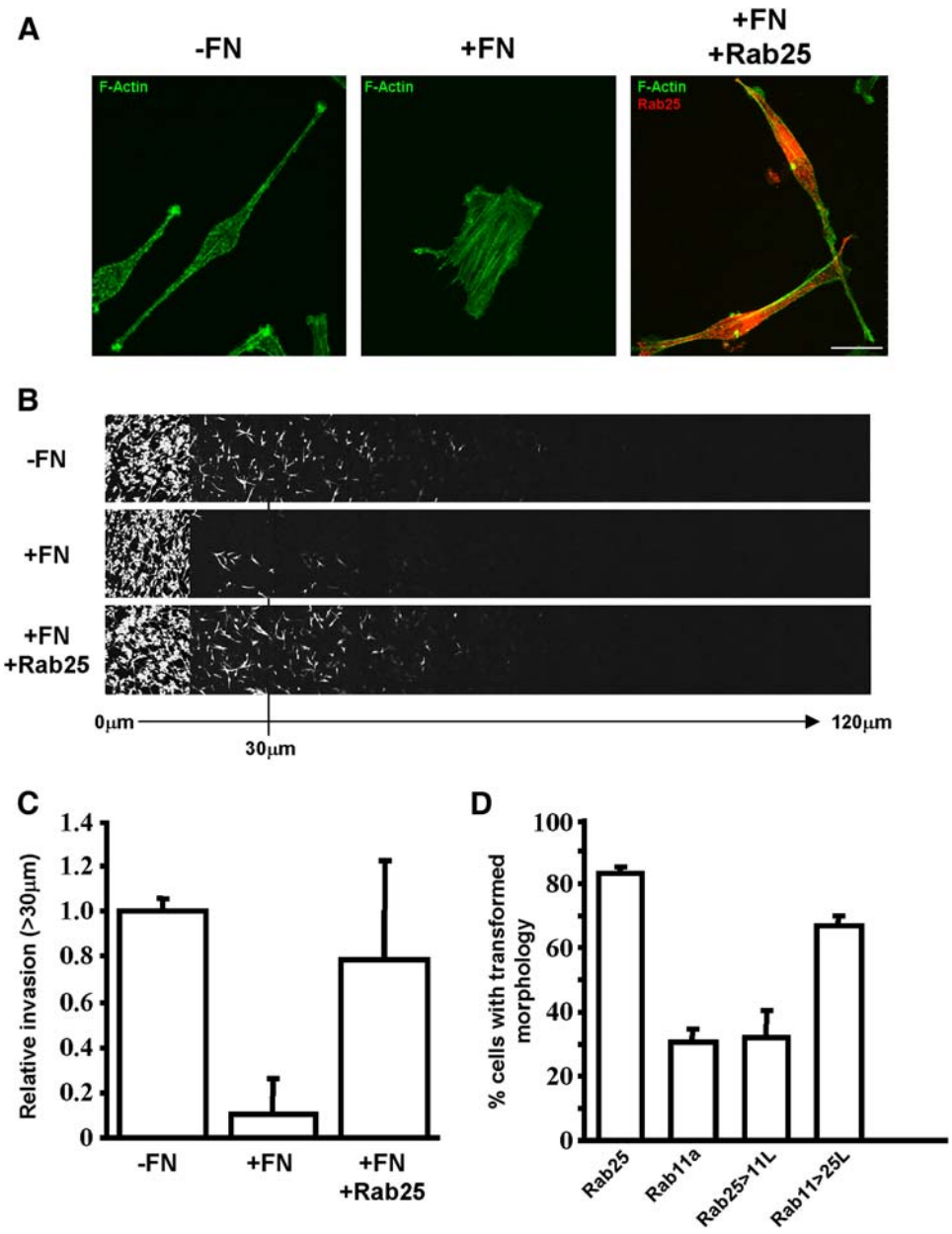

Figure 4. Rab25 Promotes Invasive Migration of v-fos-Transformed Fibroblasts in the Presence of Fibronectin

(A–D) 208F rat fibroblasts transformed with the FBR v-fos oncogene were transfected with Rab25, control vector, Rab11a, or the indicated Rab25/Rab11a domain-swap chimeras. Cells were plated on glass coverslips that were either uncoated ([A]; left panel) or fibronectin coated ([A]; middle and right panels and [D]) and were grown for 3 days prior to fixation, permeabilization, and staining for F-actin (green) and HA-Rab25 (red). The scale bar in (A) is 20 μm. The proportion of cells displaying transformed morphology (as characterized by the presence of long [>30 μm] pseudopodia) was scored and is presented in (D). Invasive migration of cells in the presence and absence of 25 μg/ml fibronectin was determined by using an inverted invasion assay. (B) Serial optical sections were captured at 15 μm intervals to a final depth 120 μm. These are presented as a sequence in which the individual optical sections are placed alongside one another with increasing depth, from left to right. (C) Cells penetrating to depths of 30 μm or greater were quantitated as in Figure 3B. Data are mean ± SEM from more than three independent experiments.

(D) A2780-Rab25 cells were transfected with control (mU6Pro-Con) and Rab25 (mU6Pro-Rab25) shRNA vectors prior to the invasion assay (left bars), or A2780-Rab25 cells were allowed to invade matrigel plugs in the presence of fibronectin (FN) and specific integrin- and FN-blocking antibodies (right bars). Cells were visualized, and data were quantitated as in (C) and were expressed relative to A2780-Rab25 cell invasion in the absence of antibody or targeting shRNA. Values are mean ± SEM from three independent experiments.

(E) Western blot demonstrating the ability of the mU6Pro-Rab25 shRNA vector to suppress the cellular levels of Rab25 protein (upper panel). Protein loading and the specificity of the RNAi were confirmed by western blot for Rab11a/b (lower panel).

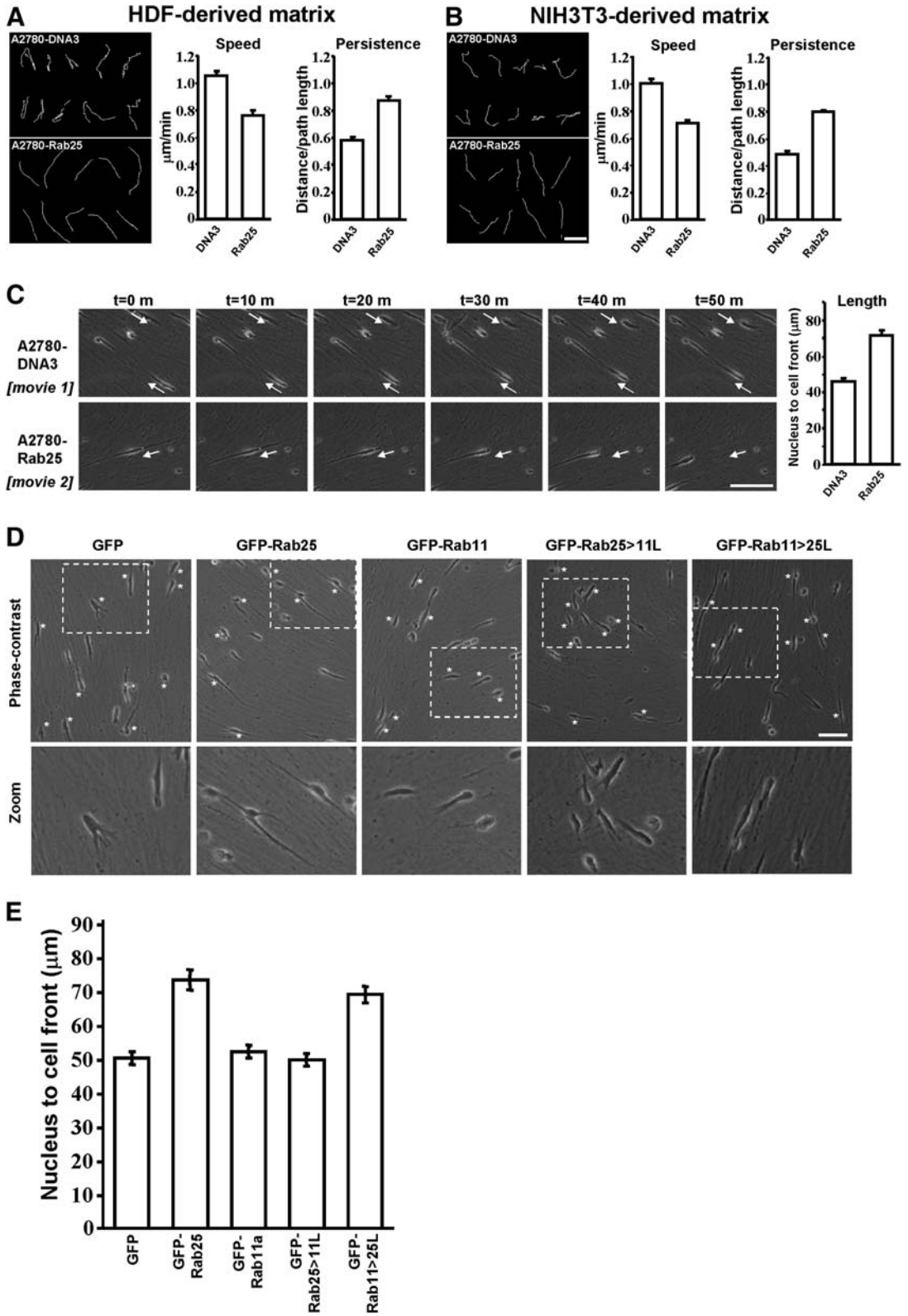

Figure 5. Rab25 Promotes Pseudopodial Migration of A2780 Cells on 3D Matrix

(A–C) A2780 cells stably expressing Rab25 or empty vector (DNA3) were plated onto matrix derived from either (A and C) human dermal fibroblasts (HDF-derived matrix) or (B) NIH 3T3 fibroblasts ~4 hr prior to time-lapse microscopy. Images were captured every 5 min over a 12 hr period, and movies were generated from these images (Movies S1 and S2). The position of the cell nucleus was followed by using cell-tracking software, and

Rab25 promoted transformed morphology even when FBR cells were plated on FN (Figure 4A) and overcame the inhibitory effect of added FN in invasive migration through matrigel (Figures 4B and 4C). Furthermore, the β1-binding mutant of Rab11, Rab11>25L, promoted transformed morphology (as determined by the presence of long [>30 μm] pseudopodia) in FBR cells plated onto FN, whereas Rab11a and Rab25>11L (which do not bind to β1) were ineffective in this regard (Figure 4D). Taken together, these data indicate that Rab25 strongly promotes invasive migration through FN-rich matrices and that it does so by associating with and regulating the function of the cell's major FN-binding integrin, α5β1.

Rab25-α5β1 Vesicles Localize to the Tips of Extending Pseudopodia during Migration on 3D Matrices

To overcome difficulties in imaging cell migration within dense 3D microenvironments, we used cell-derived matrix—a relatively thick, pliable matrix composed mainly of fibrillar collagen and FN, which recapitulates key aspects of the type of matrix found in connective tissues (Cukierman et al., 2001). A2780 cells migrated rapidly and with low persistence on cell-derived matrix (Figures 5A and 5B) and maintained an overall "slug-like" morphology as they moved (Figure 5C and Movie S1). Expression of Rab25, however, slowed the average migration speed, but it markedly increased the persistence of A2780 cell migration on matrix derived from either human dermal fibroblasts (HDF) (Figure 5A) or NIH 3T3 fibroblasts (Figure 5B), indicating that it is the persistence (and not the speed) of migration on cell-derived matrix that correlates with invasiveness under these circumstances. Moreover, Rab25-expressing cells adopted a different morphology and mode of migration that was characterized by the bilateral extension of pseudopods, followed by retraction of one process and a rapid burst of migration in the direction of the persisting pseudopod (Figure 5C and Movie S2). Contrastingly, Rab11a expression was ineffective at promoting pseudopod-driven migration, and cells continued to move with slug-like morphology after overexpression of this GTPase (Figure 5D). To obtain a quantitative index of Rab25-driven pseudopodial extension, we measured the distance between the center of the nucleus and the leading edge (in the direction of migration) and found that this increased by ~50% upon expression of HA- (Figure 5C, right panel) or GFP-tagged Rab25 (Figure 5E). Conversely, expression of GFP alone or GFP-Rab11a did not alter this index of pseudopodial morphology (Figure 5E). Crucially, expression of GFP-Rab25>11L (unable to contact β1 integrin) did not promote the extension of pseudopods, whereas Rab11>25L (does bind β1 integrin) did so (Figures 5D and 5E), indicating that acquisition of pseudopod-driven migration on pliable, 3D cell-derived matrices is dictated by the ability of the GTPase to interact with β1 integrin.

We used FLIM to determine the influence of this 3D microenvironment on Rab25-β1 association. Indeed, FRET efficiency between GFP-β1 and Cherry-Rab25 was 2-fold greater on cell-derived matrix than on glass (compare Figure 6A with Figure 1E), indicating that this 3D microenvironment strongly reinforces Rab25-integrin association within the cell. Furthermore, Cherry-Rab11a did not reduce the lifetime of GFP-β1 (Figure 6A), even though it was expressed at a similar level as Cherry-Rab25 (Figure S2), indicating that Rab11a does not bind to β1 integrin on either 2D or 3D matrices. Moreover, it appeared that association between β1 and Rab25 was particularly strong at points within pseudopodia (Figure 6A). We therefore used high-resolution time-lapse fluorescence imaging to investigate the dynamics of α5β1 and Rab25 during pseudopod-driven migration. In the absence of Rab25, GFP-α5 was localized primarily at the plasma membrane, while Cherry-Rab11a was located in the perinuclear zone (Figure 6B). Although α5 and Rab11a sometimes colocalized in the perinuclear region, vesicles transporting α5β1 were seldom seen at the cell front, and the integrin never colocalized with Rab11a in the anterior portion of the cell (Figure 6B′ and Movie S3). Upon expression of Cherry-Rab25, vesicles containing both the integrin and Rab25 clearly colocalized in pseudopodial tips (Figures 6C, 6C′, and 6D). Furthermore, Rab25-α5β1 vesicles were slow-moving structures (Movie S4), whereas vesicles carrying the integrin alone moved more rapidly and were often seen to be transported rapidly backward toward the cell body (not shown).

Rab25 Vesicles Deliver α5β1 Integrin to the Plasma Membrane at Pseudopodial Tips

We employed photoactivation in combination with time-lapse microscopy to resolve whether Rab25-α5β1 vesicles in pseudopodia are involved in recycling integrin to the plasma membrane. A2780 cells expressing photoactivatable paGFP-α5 integrin and Cherry-Rab25 were plated onto cell-derived matrix. A pulse of 405 nm laser light aimed at a "single point" corresponding to a Rab25-positive vesicle resulted in near-immediate photoactivation of paGFP-α5 integrin within the confines of this structure (Figure 7A). During the following 60 s, fluorescence was lost from the photoactivated vesicle, and this was

representative examples of migration tracks are displayed. The scale bar in (B) is 200 μm. Stills from these movies corresponding to 10 min intervals are presented in (C). Arrows indicate the position of the cell(s) at the start of the movie. The scale bar in (C) is 100 μm.

(D) A2780 cells expressing GFP, GFP-Rab25, GFP-Rab11a, GFP-Rab25>11L, or GFP-Rab11>25L were seeded onto cell-derived matrix. A total of 12 hr after seeding, fluorescence and phase-contrast images were captured. Only the phase-contrast images are presented; the asterisk indicates cells expressing GFP or a GFP fusion. The scale bar is 100 μm.

(E) The distance between the center of the nucleus and the cell front (with respect to the direction of migration) for cells treated as described in (D) was measured by using ImageJ. Data represent mean ± SEM, n > 150 cells.

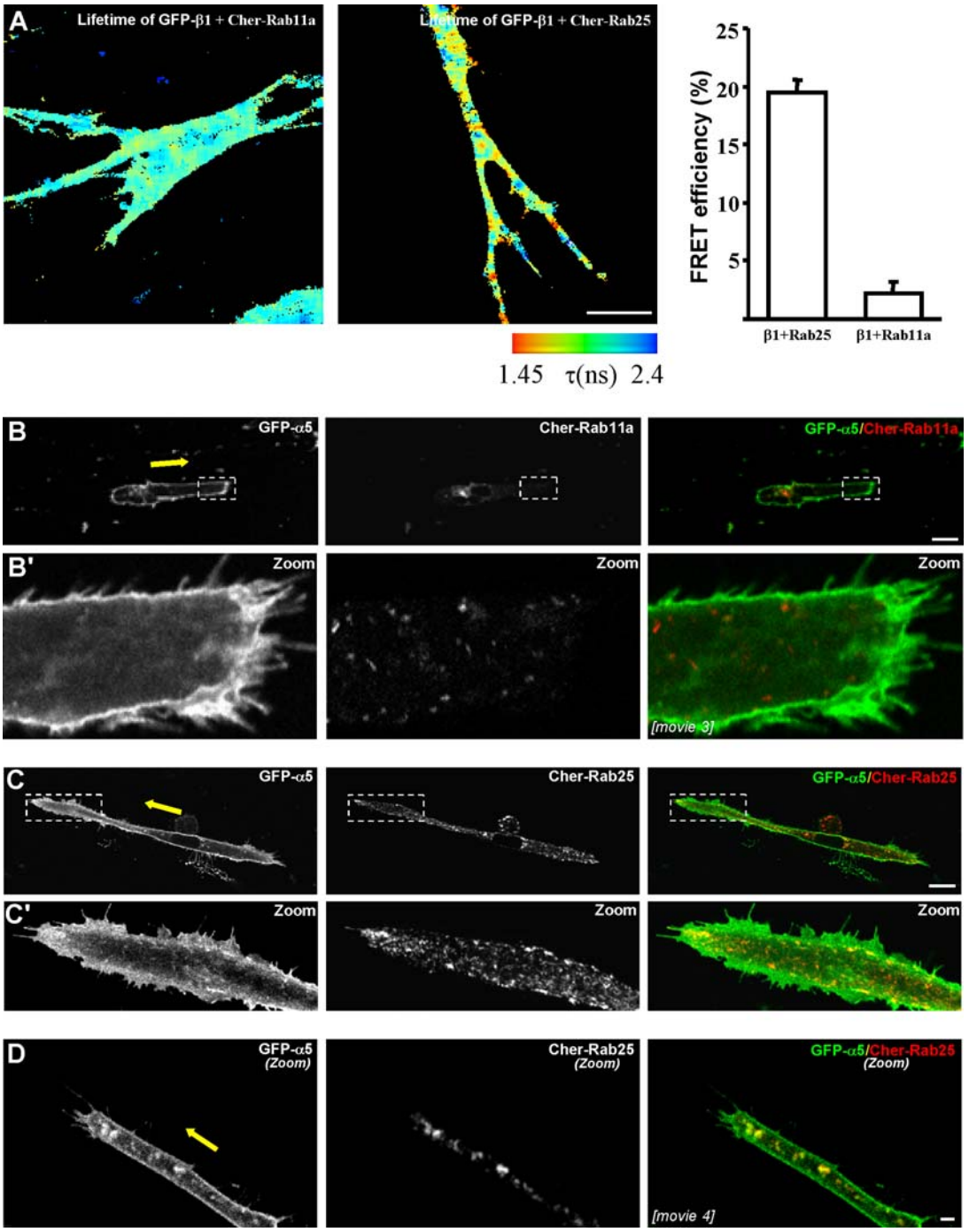

Figure 6. Rab25-α5β1 Vesicles Are Localized to Pseudopods during Migration on 3D Matrix

(A) β1 −/− fibroblasts expressing GFP-β1 integrin were transfected with Cherry-Rab25 or -Rab11a and were plated onto HDF-derived matrices. Lifetime images mapping spatial FRET across the cells are depicted with a pseudocolor scale (blue, normal lifetime; red, FRET). The scale bar is 20 μm. The graph depicts FRET efficiency over three independent experiments. Values are mean ± SEM, n = 10.

(B–D) A2780 cells expressing GFP-α5 and (B) Cherry-Rab11a or (C and D) Cherry-Rab25 were plated onto HDF-derived matrix in glass-bottomed dishes and imaged with confocal microscopy. Images were captured at 1.0–1.5 frames/s over a period of 30–40 s, and movies were generated from these images (Movies S3 and S4). Single-section confocal image stills corresponding to an individual frame from these movies are presented. The scale bars in (B) and (C) are 10 μm; the scale bar in (D) is 1 μm. The yellow arrows indicate the direction of migration. The images within the dotted squares are shown enlarged in (B′) and (C′) (zoom) as appropriate.

accompanied by a concerted and concomitant appearance of the fluorophore at the plasma membrane around the pseudopodial tip (Figures 7A and 7C and Movie S5). Conversely, when an activating single point was aimed at a region without a Rab25 vesicle, little or no photoactivation was detected (although subsequent activation of a larger region confirmed the expression of paGFP-α5) (Figure 7B), indicating that the integrin visible in Figure 7A is indeed at a Rab25 vesicle, and not at the plasma membrane above and below this. Moreover, in cells expressing a farnesyl-tagged paGFP (paGFP^{farn}, a lipid-anchored paGFP used as a reporter of plasma membrane dynamics), which is localized primarily to the plasma membrane (and never to Rab25 vesicles), little or no fluorescence was detectable when using this single-point photoactivation protocol (not shown). Taken together, these data indicate that the pool of α5β1 integrin at Rab25 vesicles is neither static nor sequestered within these structures, but that it is being continuously recycled to the plasma membrane at pseudopodial tips.

Rab25 Acts to Retain a Pool of α5β1 at Pseudopodial Tips

Rab25 promotes a more persistent mode of tumor-cell migration on cell-derived matrix and stabilizes pseudopods in a way that is dependent on its ability to bind to β1 integrin. Given that the Rab25 vesicles in pseudopods are involved in delivering integrin to the distal plasma membrane, it is possible that Rab25 may contribute to invasion by maintaining a discrete pool of integrin within the pseudopodial compartment. We addressed this by photoactivating α5β1 at the front of cells migrating on cell-derived matrix and by following the dynamics of this population of integrin heterodimers. In A2780 cells expressing Cherry-Rab11a, a patch of α5β1 integrin photoactivated at the cell front was seen to disperse from this region over the following 2 min (Figure 7D, Figure S3A, and Movie S6). However, in Rab25-expressing cells, much more of this anteriorly located α5β1 remained within the photoactivated region (at vesicles and at the distal plasma membrane) over the same time period (Figure 7E, Figure S3A, and Movie S7). Moreover, photoactivated paGFP^{farn} dispersed from the cell front irrespective of expression of Rab25 or Rab11a (Figure S3A). To correct for photobleaching, we expressed the data in Figure S2A as a function of those in Figure S3B. This revealed that, in the absence of Rab25, paGFP-α5 and paGFP^{farn} fluorescence were lost from the cell front at similar rates (Figure 7F). Moreover, Rab25 did not alter the rate at which paGFP^{farn} fluorescence was lost from the pseudopod, indicating that this GTPase does not change the fluidity of the plasma membrane at the cell front (Figure 7F). However, the bulk of paGFP-α5 was very effectively retained at the cell front by expression of Rab25 (Figure 7F). Taken together, these data indicate that, although α5β1 is normally free to diffuse from the cell front with the same kinetics as a marker of overall plasma membrane fluidity, upon expression of Rab25 a discrete pool of integrin is efficiently retained at the pseudopodial tip.

DISCUSSION

Here, we have detailed a direct interaction between the cytodomain of β1 integrin and a Rab11-family GTPase, Rab25, which strongly promotes a pseudopodial/invasive mode of cell migration both across and through 3D FN-containing matrices, and we note that this appears to be mediated by the ability of the GTPase to localize a discrete pool of actively cycling α5β1 to the tips of invading pseudopodia.

Clinical studies demonstrate that Rab25 increases the aggressiveness of breast and ovarian cancers (Cheng et al., 2004), and this may be due to modulation of cellular processes such as proliferation, survival, and migration. Rab25 has been reported to increase anchorage-independent growth and colony-forming activity in A2780 cells, indicating that proapoptotic signals are suppressed by Rab25 (Cheng et al., 2004). Indeed, we find that while Rab25 does not affect A2780 cell proliferation (Figure S4), Rab25-expressing cells remain viable for an extended period of time after reaching confluence (Figure S5). However, the α5β1- and FN-blocking antibodies that ablate invasiveness do not oppose Rab25-mediated survival (Figure S5), indicating that the GTPase can provide survival cues independently of α5β1 and FN. Thus, Rab25 can promote cell survival, and although the mechanisms for this will be of interest, they are quite distinct from those that drive invasive migration of tumor cells.

A number of β subunit integrin interactions have been documented, and their functional implications range from acting as signaling adaptors (p120^{FAK} and paxillin), to linking integrins to the actin cytoskeleton (α-actinin, filamin, and talin), and to regulating integrin endocytic recycling (PKD1) and the ability of talin to switch integrins from the inactive to the active conformation (inside-out activation)—a phenomenon that is now well characterized at the molecular level (Otey et al., 1990; Tadokoro et al., 2003; White et al., 2007; Woods et al., 2004; Wegener et al., 2007). Although we find that β1 integrin surface expression (Figure S6) and its activation status (Figure S7) are unaltered by Rab25, the GTPase clearly controls the dynamics of α5β1 at the cell front, indicating that the primary role of the Rab25-integrin association is to maintain a pool of actively recycling heterodimer within invading pseudopods, and not to regulate inside-out signaling.

Early models of integrin trafficking favored a mechanism by which integrins were internalized at the rear of the cell, transported forward within vesicles toward the lammellipodium, and then exocytosed at the leading edge. Evidence to support this model, however, has not been forthcoming. Indeed, it appears more likely that both integrin endocytosis and exocytosis occur at the leading edge (Caswell and Norman, 2006), and that models invoking bulk anterograde flow of integrin vesicles into the

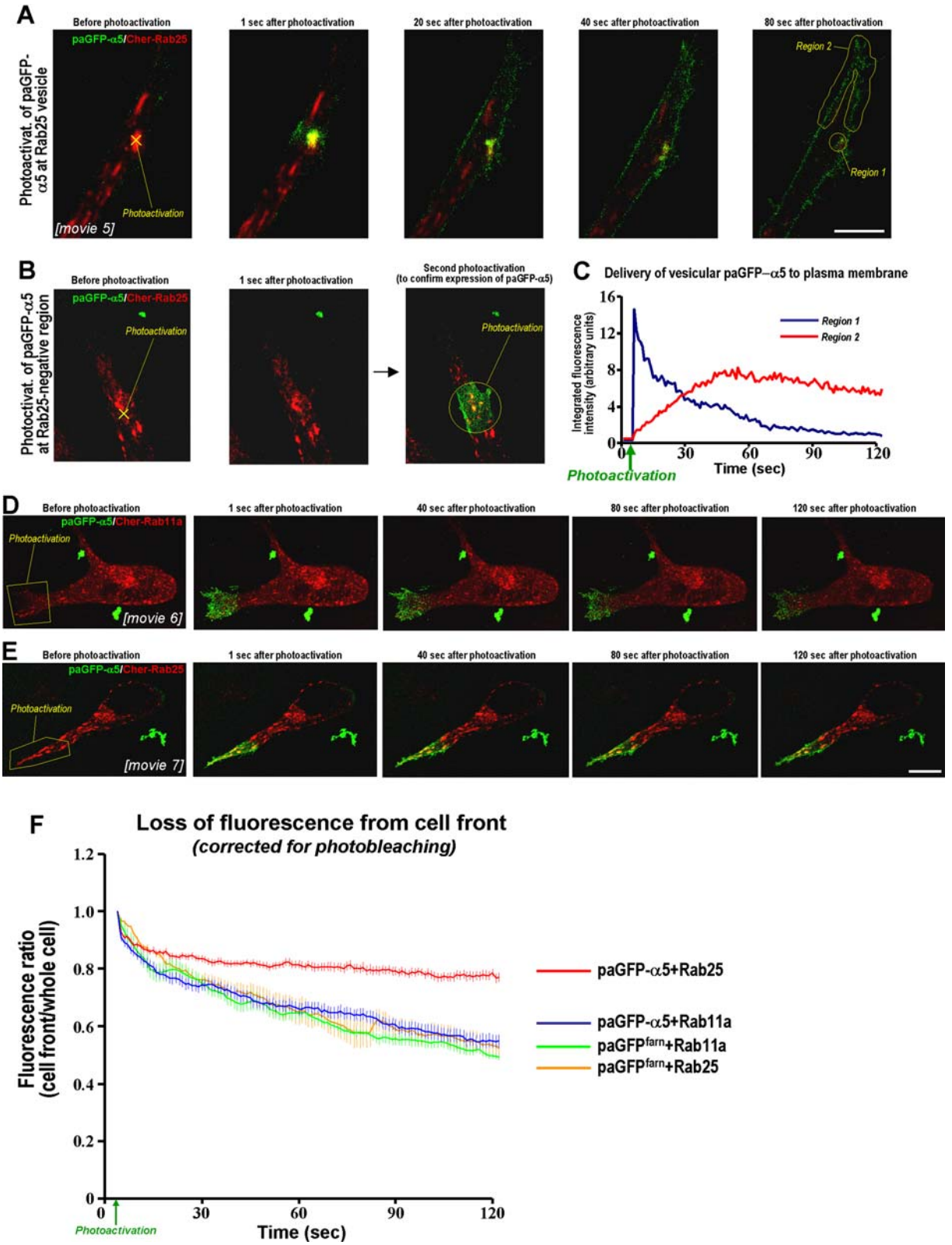

Figure 7. Photoactivation/Fluorescence Time-Lapse Analysis of α5β1 Integrin Dynamics during Migration on 3D Matrix

(A–C) A2780 cells expressing photoactivatable α5 integrin (paGFP-α5; green) and Cherry-Rab25 (red) were plated onto HDF-derived matrix and imaged by confocal microscopy. Photoactivation was achieved with a 405 nm laser aimed at a "single point" corresponding to either (A) a Rab25 vesicle or (B) a region not containing Rab25, as indicated by the yellow crosses. Images were then captured at 1 frame/s over a period of 120 s,

lammellipod may not be correct. Indeed, we do not see any net flux of α5β1 vesicles from the rear to the front of migrating cells, nor do we detect anterograde movement of vesicles from the perinuclear region to the pseudopod. We do, however, occasionally observe what appear to be endocytic vesicles that form near the cell front and then carry α5β1 rapidly backward; however, crucially, these endosomes never contain Rab25. More importantly, we consistently observe Rab25-α5β1-containing vesicles/endosomes localized to the distal regions of pseudopods. However, single-point photactivation experiments (Figure 7A) indicate that these Rab25-positive vesicles do not contain a static or "sequestered" pool of α5β1, but are continuously delivering integrin to the plasma membrane at the cell front. Notwithstanding, it is important to note that when the whole pseudopodial tip (vesicles and plasma membrane) is photoactivated (Figure 7E), the quantity of fluorescent integrin within Rab25 vesicles does not appreciably diminish, indicating that these structures are replenished with α5β1 from within the photoactivated region. We therefore favor a mechanism in which α5β1 is rapidly internalized and recycled in the extreme anterior portion of the cell, and we find that this process acts to maintain a discrete pool of integrin at the pseudopodial tip. Rab25 may provide the platform on which this mechanism is hinged, and it may promote the localization of α5β1 within the pseudopod, prevent retrograde traffic, and thus contribute to pseudopod stability. Myosins are known to associate with Rab proteins via bridging molecules. For example, Rab27 associates with MyoVa through an interaction with melanophilin or with MyoVIIa through Myosin- and Rab-interacting protein (MyRIP), and Rab11-family members (including Rab25) are known to associate with MyoVb, an association that is probably bridged by the Rab11 "effector" Rab11-FIP2 (Seabra and Coudrier, 2004). Rab27 is thought to contribute to the peripheral accumulation of melanosomes by enabling their MyoVa-dependant capture within the distal, actin-rich regions of melanocyte dendritic processes. Preliminary coimmunoprecipitation experiments indicate that Rab25 bridges a physical interaction between α5β1 and FIP2, leading to the intriguing possibility that Rab25 acts through FIP2 to recruit MyoVb to Rab25-α5β1 vesicles and thus capture the integrin at the tips of extending pseudopods, where these vesicles deliver their integrin cargo to the plasma membrane by exocytosis.

In conclusion, our results demonstrate that Rab25 interacts directly with α5β1 integrin and promotes invasive, metastatic-like migration through FN-rich matrices that is likely mediated by the GTPase acting to localize vesicular α5β1 to the tips of extending pseudopods; this α5β1 can then be exchanged with the plasma membrane within this locale. A number of studies have found that antibodies and other agents that target α5β1 integrin may oppose metastasis (Humphries et al., 1986; Qian et al., 2005), and, indeed, anti-α5β1 drugs will soon be available for clinical use. However, the fact that the α5β1-FN ligand pair is known to have both stimulatory and inhibitory effects on tumorogenesis (Hynes, 1976; Spence et al., 2006; Vaheri and Mosher, 1978; Yamada and Olden, 1978) may lead to mixed results in clinical trials. Our observation that Rab25 can act in conjunction with α5β1 to favor an invasive phenotype suggests that this GTPase may be used as a biomarker, which would allow for the selection of patients who are likely to respond to anti-α5β1-FN targeted therapies. In fact, given the identification of both Rab25 and β1 integrin as key components of the invasive carcinoma gene expression signature (Wang et al., 2004), the direct interaction between Rab25 and β1 integrin may in itself be a therapeutic target.

EXPERIMENTAL PROCEDURES

Cell Culture and Transfection

Stable clones of A2780-DNA3 and A2780-Rab25 cells were generated as described previously (Cheng et al., 2004). A2780 cells were maintained in RPMI supplemented with 10% (v/v) serum at 37°C and 10% CO_2. Transfection of shRNAi vectors was carried out by using the Amaxa "Nucleofector" system (solution T, program A-23) according to the manufacturer's instructions. COS-1 cells were maintained in DMEM supplemented with 10% (v/v) serum at 37°C and 10% CO_2. COS-1 cells were transfected by using FuGENE according to the manufacturer's instructions. 208F rat fibroblasts transformed with the FBR v-fos oncogene were obtained from Tom Curran. 208F cells were maintained in DMEM supplemented with 10% serum at 37°C and 10% CO_2 and were transfected by using the Amaxa "Nucleofector" system (solution R, program T-20) according to the manufacturer's instructions.

Immunoprecipitations

A2780 cells were lysed in lysis buffer (200 mM NaCl, 75 mM Tris-HCl [pH 7], 15 mM NaF, 1.5 mM Na_3VO_4, 7.5 mM EDTA, 7.5 mM EGTA,

and movies were generated from these images (Movie S5); single-section confocal image stills corresponding to individual frames from one of these movies are presented. The scale bar in (A) is 5 μm. The integrated fluorescence intensity of regions 1 and 2 (as depicted in [A], right panel) was quantified for each frame of Movie S5, and these values are plotted against time in (C).

(D and E) A2780 cells expressing photoactivatable paGFP-α5 (green) and either (D) Cherry-Rab11a (red) or (E) Cherry-Rab25 (red) were plated onto HDF-derived matrix and imaged by confocal microscopy. paGFP-α5 was photoactivated within the indicated regions at the front of the cell; images were then captured, and movies were generated (Movies S6 and S7). Confocal stills are presented as for (A) The scale bar in (E) is 10 μm.

(F) Cells expressing photoactivatable paGFP-α5 or farnesylated photoactivatable GFP (paGFP^{farn}) in combination with either Cherry-Rab11a or Cherry-Rab25 were plated onto HDF-derived matrix. The photoactivation region was selected to be at the cell front, as indicated in (D) and (E), and movies were generated as described in (A). The integrated fluorescence intensity of the photoactivated region (see Figure S3A) was quantified for each frame of these movies, calculated relative to the intensity of the frame immediately after photoactivation, corrected for photobleaching (by expressing the values in Figure S3A as a function of those in Figure S3B), and plotted against time. Values are mean fluorescence intensity over three individual experiments ± SEM; n = 20 for paGFP-α5, and n = 6 for paGFP^{farn}.

0.15% [v/v] Tween 20, 50 μg/ml leupeptin, 50 μg/ml aprotinin, and 1 mM 4-(2-aminoethyl)-benzenesulfonyl fluoride). Lysates were passed three times through a 27-gauge needle and clarified by centrifugation at 10,000 × g for 10 min at 4°C. Magnetic beads conjugated to sheep anti-mouse IgG were bound to anti-integrin, anti-HA, or anti-GFP monoclonal antibodies. Antibody-coated beads were incubated with lysates for 2 hr at 4°C with constant rotation. Unbound proteins were removed by extensive washing in lysis buffer, and specifically associated proteins were eluted from the beads by boiling for 10 min in Laemmli sample buffer. Proteins were resolved by SDS-PAGE and analyzed by western blot as described previously (Norman et al., 1998).

GST Pull-Down Assay

Glutathione-agarose beads were bound to purified bacterially expressed GST fusion proteins. Lysates of COS-1 cells overexpressing HA-Rab25 were incubated with GST fusion-coated agarose beads for 2 hr at 4°C. To determine whether Rab25 and β1 integrin interact directly, His-Rab25 was expressed in *Escherichia coli* stain BL-21 and purified by sequential Ni-affinity and size-exclusion chromatography. His-Rab25 was nucleotide loaded by incubation in PBS containing 4.3 mM EDTA and 0.11 mM GDP or GTPγS for 1 hr at room temperature. His-Rab25 was subsequently diluted 1:3 in PBS, and $MgCl_2$ was added to a final concentration of 6.5 mM to maintain the GTPase in its nucleotide-loaded state. GDP- and GTPγS-loaded His-Rab25 were diluted 1:10 in PBS and incubated with GST fusion-coated beads for 2 hr at 4°C with constant rotation. Unbound proteins were removed by extensive washing in lysis buffer, and specifically associated proteins were eluted from the beads by boiling for 10 min in Laemmli sample buffer. Proteins were resolved by SDS-PAGE and analyzed by Coomassie staining and western blot.

Inverted Invasion Assay

Inverted invasion assays were performed as described previously (Hennigan et al., 1994). Briefly, matrigel or Collagen I (mixed 4:1 with 5× RPMI) supplemented with 25 μg/ml FN as indicated was allowed to polymerize in transwell inserts (Corning) for 1 hr at 37°C. Inserts were then inverted, and cells were seeded directly onto the opposite face of the filter. Transwell inserts were finally placed in serum-free medium, and medium supplemented with 10% FCS (208F cells) or 10% FCS and 30 ng/ml EGF (A2780 cells) was placed on top of the matrix, providing a chemotactic gradient. Where appropriate, integrin/FN-blocking antibodies were added to the matrigel prior to plug polymerization at a concentration of 1 μg/ml, and they were also added to the medium throughout the system. Between 48 and 72 hr after seeding, invading cells were stained with Calcein-AM and visualized by confocal microscopy; serial optical sections were captured at 15 μm intervals.

Generation of Cell-Derived Matrix

Cell-derived matrix was generated as described previously (Bass et al., 2007; Cukierman et al., 2001). Briefly, gelatin-coated tissue culture-ware was crosslinked with glutaraldehyde, quenched, and equilibrated in DMEM containing 10% FCS. Primary cultured human dermal fibroblasts (HDFs) or NIH 3T3 fibroblasts were seeded at near confluence (~2×10^4 cells/cm^2) and grown for 10 days (HDFs) or 8 days (NIH 3T3s) in DMEM containing 10% FCS and 50 μg/ml ascorbic acid. Matrices were denuded of living cells by incubation with PBS containing 20 mM NH_4OH and 0.5% Triton X-100, and DNA residue was removed by incubation with DNaseI. Matrices were blocked with 0.1% heat-denatured BSA prior to seeding of cells.

Time-Lapse Microscopy on Cell-Derived Matrix

A2780 cells were seeded onto cell-derived matrix-coated 6-well plates or glass-bottomed 3 cm plates and were incubated at 37°C until cells adhered and began migrating (>4 hr). Cells were imaged with a 10× objective and an inverted microscope (Axiovert S100, Carl Zeiss MicroImaging, Inc.) in an atmosphere of 5% CO_2 at 37°C or with a 64× objective and an inverted confocal microscope (Fluoview FV1000, Olympus) in an atmosphere of 5% CO_2 at 37°C. Photoactivation of paGFP was achieved by using a 405 nm laser with an Olympus FV-100 inverted microscope and an Olympus SIM scanner.

Fluorescence Lifetime Measurements by Time-Correlated Single Photon Counting FLIM

The methods for derivation of β1 integrin −/− mouse embryo fibroblasts in which the FLIM experiments were performed are described in Supplemental Experimental Procedures. Time-domain FLIM was performed with a multiphoton microscope system as described previously (Parsons et al., 2005). Briefly, the system is based on a modified Bio-Rad MRC 1024MP workstation, comprised of a solid-state-pumped femtosecond Ti:Sapphire (Tsunami, Spectra-Physics) laser system, a focal scan-head, and an inverted microscope (Nikon TE200). Enhanced detection of the scattered component of the emitted (fluorescence) photons was afforded by the use of fast-response (Hamamatsu R7401-P), nondescanned detectors, developed in house, situated in the reimaged objective pupil plane. Fluorescence lifetime imaging capability was provided by time-correlated single-photon counting electronics (Becker & Hickl, SPC 700). A 40× objective was used throughout (Nikon, CFI60 Plan Fluor N.A. 1.3), and data were collected at 500 ± 20 nm through a bandpass filter (Coherent, Inc. 35-5040). Widefield acceptor (mRFP) images were acquired with a CCD camera (Hammamatsu) at < 200 ms exposure times.

Supplemental Data

The Supplemental Data include a full description of the materials and DNA constructs used, the generation of β1−/− cells, and a detailed procedure for the analysis of the FRET/FLIM experiments, and can be found with this article online at http://www.developmentalcell.com/cgi/content/full/13/4/496/DC1/.

ACKNOWLEDGMENTS

This work was supported by Cancer Research United Kingdom. M.W.M. was supported by a Science Foundation Ireland investigator grant (05/IN.3/B 859). We thank M. O'Prey and T. Gilbey for assistance with microscopy. We also thank Ken Yamada, Donna Webb, Jennifer Lippincott-Schwartz, and Juliana Schwarz for the generous gifts of reagents, and Mr. Bass for his invaluable assistance with the method for making cell-derived matrix.

Received: July 25, 2006
Revised: June 1, 2007
Accepted: August 27, 2007
Published: October 9, 2007

REFERENCES

Akiyama, S.K., Olden, K., and Yamada, K.M. (1995). Fibronectin and integrins in invasion and metastasis. Cancer Metastasis Rev. *14*, 173–189.

Bass, M.D., Roach, K.A., Morgan, M.R., Mostafavi-Pour, Z., Schoen, T., Muramatsu, T., Mayer, U., Ballestrem, C., Spatz, J.P., and Humphries, M.J. (2007). Syndecan-4-dependent Rac1 regulation determines directional migration in response to the extracellular matrix. J. Cell Biol. *177*, 527–538.

Caswell, P.T., and Norman, J.C. (2006). Integrin trafficking and the control of cell migration. Traffic *7*, 14–21.

Cheng, K.W., Lahad, J.P., Kuo, W.L., Lapuk, A., Yamada, K., Auersperg, N., Liu, J., Smith-McCune, K., Lu, K.H., Fishman, D., et al. (2004). The RAB25 small GTPase determines aggressiveness of ovarian and breast cancers. Nat. Med. *10*, 1251–1256.

Cukierman, E., Pankov, R., Stevens, D.R., and Yamada, K.M. (2001). Taking cell-matrix adhesions to the third dimension. Science *294*, 1708–1712.

Curran, T., and Verma, I.M. (1984). FBR murine osteosarcoma virus. I. Molecular analysis and characterization of a 75,000-Da gag-fos fusion product. Virology *135*, 218–228.

Danen, E.H., and Yamada, K.M. (2001). Fibronectin, integrins, and growth control. J. Cell. Physiol. *189*, 1–13.

Even-Ram, S., and Yamada, K.M. (2005). Cell migration in 3D matrix. Curr. Opin. Cell Biol. *17*, 524–532.

Fabbri, M., Di Meglio, S., Gagliani, M.C., Consonni, E., Molteni, R., Bender, J.R., Tacchetti, C., and Pardi, R. (2005). Dynamic partitioning into lipid rafts controls the endo-exocytic cycle of the αL/β2 integrin, LFA-1, during leukocyte chemotaxis. Mol. Biol. Cell *16*, 5793–5803.

Garcia, M.J., Pole, J.C., Chin, S.F., Teschendorff, A., Naderi, A., Ozdag, H., Vias, M., Kranjac, T., Subkhankulova, T., Paish, C., et al. (2005). A 1 Mb minimal amplicon at 8p11–12 in breast cancer identifies new candidate oncogenes. Oncogene *24*, 5235–5245.

Gebhardt, C., Breitenbach, U., Richter, K.H., Furstenberger, G., Mauch, C., Angel, P., and Hess, J. (2005). c-Fos-dependent induction of the small ras-related GTPase Rab11a in skin carcinogenesis. Am. J. Pathol. *167*, 243–253.

Goldenring, J.R., Shen, K.R., Vaughan, H.D., and Modlin, I.M. (1993). Identification of a small GTP-binding protein, Rab25, expressed in the gastrointestinal mucosa, kidney, and lung. J. Biol. Chem. *268*, 18419–18422.

Gress, T.M., Muller-Pillasch, F., Geng, M., Zimmerhackl, F., Zehetner, G., Friess, H., Buchler, M., Adler, G., and Lehrach, H. (1996). A pancreatic cancer-specific expression profile. Oncogene *13*, 1819–1830.

Hennigan, R.F., Hawker, K.L., and Ozanne, B.W. (1994). Fos-transformation activates genes associated with invasion. Oncogene *9*, 3591–3600.

Humphries, M.J., Olden, K., and Yamada, K.M. (1986). A synthetic peptide from fibronectin inhibits experimental metastasis of murine melanoma cells. Science *233*, 467–470.

Hynes, R.O. (1976). Cell surface proteins and malignant transformation. Biochim. Biophys. Acta *458*, 73–107.

Hynes, R.O. (2002). Integrins: bidirectional, allosteric signaling machines. Cell *110*, 673–687.

Jones, M.C., Caswell, P.T., and Norman, J.C. (2006). Endocytic recycling pathways: emerging regulators of cell migration. Curr. Opin. Cell Biol. *18*, 549–557.

McGarry, L.C., Winnie, J.N., and Ozanne, B.W. (2004). Invasion of v-Fos(FBR)-transformed cells is dependent upon histone deacetylase activity and suppression of histone deacetylase regulated genes. Oncogene *23*, 5284–5292.

Natrajan, R., Williams, R.D., Hing, S.N., Mackay, A., Reis-Filho, J.S., Fenwick, K., Iravani, M., Valgeirsson, H., Grigoriadis, A., Langford, C.F., et al. (2006). Array CGH profiling of favourable histology Wilms tumours reveals novel gains and losses associated with relapse. J. Pathol. *210*, 49–58.

Norman, J.C., Jones, D., Barry, S.T., Holt, M.R., Cockcroft, S., and Critchley, D.R. (1998). ARF1 mediates paxillin recruitment to focal adhesions and potentiates Rho-stimulated stress fiber formation in intact and permeabilized Swiss 3T3 fibroblasts. J. Cell Biol. *143*, 1981–1995.

Otey, C.A., Pavalko, F.M., and Burridge, K. (1990). An interaction between α-actinin and the β 1 integrin subunit in vitro. J. Cell Biol. *111*, 721–729.

Pankov, R., Cukierman, E., Katz, B.Z., Matsumoto, K., Lin, D.C., Lin, S., Hahn, C., and Yamada, K.M. (2000). Integrin dynamics and matrix assembly: tension-dependent translocation of α(5)β(1) integrins promotes early fibronectin fibrillogenesis. J. Cell Biol. *148*, 1075–1090.

Parsons, M., Monypenny, J., Ameer-Beg, S.M., Millard, T.H., Machesky, L.M., Peter, M., Keppler, M.D., Schiavo, G., Watson, R., Chernoff, J., et al. (2005). Spatially distinct binding of Cdc42 to PAK1 and N-WASP in breast carcinoma cells. Mol. Cell. Biol. *25*, 1680–1695.

Pellinen, T., Arjonen, A., Vuoriluoto, K., Kallio, K., Fransen, J.A., and Ivaska, J. (2006). Small GTPase Rab21 regulates cell adhesion and controls endosomal traffic of {β}1-integrins. J. Cell Biol. *173*, 767–780.

Powelka, A.M., Sun, J., Li, J., Gao, M., Shaw, L.M., Sonnenberg, A., and Hsu, V.W. (2004). Stimulation-dependent recycling of integrin β1 regulated by ARF6 and Rab11. Traffic *5*, 20–36.

Qian, F., Zhang, Z.C., Wu, X.F., Li, Y.P., and Xu, Q. (2005). Interaction between integrin α(5) and fibronectin is required for metastasis of B16F10 melanoma cells. Biochem. Biophys. Res. Commun. *333*, 1269–1275.

Ray, G.S., Lee, J.R., Nwokeji, K., Mills, L.R., and Goldenring, J.R. (1997). Increased immunoreactivity for Rab11, a small GTP-binding protein, in low-grade dysplastic Barrett's epithelia. Lab. Invest. *77*, 503–511.

Ray, M.E., Yang, Z.Q., Albertson, D., Kleer, C.G., Washburn, J.G., Macoska, J.A., and Ethier, S.P. (2004). Genomic and expression analysis of the 8p11–12 amplicon in human breast cancer cell lines. Cancer Res. *64*, 40–47.

Roberts, M., Barry, S., Woods, A., van der Sluijs, P., and Norman, J. (2001). PDGF-regulated rab4-dependent recycling of α v β 3 integrin from early endosomes is necessary for cell adhesion and spreading. Curr. Biol. *11*, 1392–1402.

Roberts, M.S., Woods, A.J., Dale, T.C., Van Der Sluijs, P., and Norman, J.C. (2004). Protein kinase B/Akt acts via glycogen synthase kinase 3 to regulate recycling of α v β 3 and α 5 β 1 integrins. Mol. Cell. Biol. *24*, 1505–1515.

Seabra, M.C., and Coudrier, E. (2004). Rab GTPases and myosin motors in organelle motility. Traffic *5*, 393–399.

Spence, H.J., McGarry, L., Chew, C.S., Carragher, N.O., Scott-Carragher, L.A., Yuan, Z., Croft, D.R., Olson, M.F., Frame, M., and Ozanne, B.W. (2006). AP-1 differentially expressed proteins Krp1 and fibronectin cooperatively enhance Rho-ROCK-independent mesenchymal invasion by altering the function, localization, and activity of nondifferentially expressed proteins. Mol. Cell. Biol. *26*, 1480–1495.

Strachan, L.R., and Condic, M.L. (2004). Cranial neural crest recycle surface integrins in a substratum-dependent manner to promote rapid motility. J. Cell Biol. *167*, 545–554.

Tadokoro, S., Shattil, S.J., Eto, K., Tai, V., Liddington, R.C., de Pereda, J.M., Ginsberg, M.H., and Calderwood, D.A. (2003). Talin binding to integrin β tails: a final common step in integrin activation. Science *302*, 103–106.

Vaheri, A., and Mosher, D.F. (1978). High molecular weight, cell surface-associated glycoprotein (fibronectin) lost in malignant transformation. Biochim. Biophys. Acta *516*, 1–25.

Wang, W., Goswami, S., Lapidus, K., Wells, A.L., Wyckoff, J.B., Sahai, E., Singer, R.H., Segall, J.E., and Condeelis, J.S. (2004). Identification and testing of a gene expression signature of invasive carcinoma cells within primary mammary tumors. Cancer Res. *64*, 8585–8594.

Wegener, K.L., Partridge, A.W., Han, J., Pickford, A.R., Liddington, R.C., Ginsberg, M.H., and Campbell, I.D. (2007). Structural basis of integrin activation by talin. Cell *128*, 171–182.

White, D.P., Caswell, P.T., and Norman, J.C. (2007). {α}v{β}3 and {α}5{β}1 integrin recycling pathways dictate downstream Rho kinase signaling to regulate persistent cell migration. J. Cell Biol. *177*, 515–525.

Woods, A.J., White, D.P., Caswell, P.T., and Norman, J.C. (2004). PKD1/PKCmu promotes αvβ3 integrin recycling and delivery to nascent focal adhesions. EMBO J. *23*, 2531–2543.

Yamada, K.M., and Olden, K. (1978). Fibronectins–adhesive glycoproteins of cell surface and blood. Nature *275*, 179–184.

Yoon, S.O., Shin, S., and Mercurio, A.M. (2005). Hypoxia stimulates carcinoma invasion by stabilizing microtubules and promoting the Rab11 trafficking of the α6β4 integrin. Cancer Res. *65*, 2761–2769.

Zamir, E., Katz, B.Z., Aota, S., Yamada, K.M., Geiger, B., and Kam, Z. (1999). Molecular diversity of cell-matrix adhesions. J. Cell Sci. *112*, 1655–1669.

Zerial, M., and McBride, H. (2001). Rab proteins as membrane organizers. Nat. Rev. Mol. Cell Biol. *2*, 107–117.